Left Ventricular Assist Devices: Impact of Flow Ratios on The Localisation of Cardiovascular Diseases Using Computational Fluid Dynamics

DOI:
10.1016/j.procir.2015.11.008

Available online at www.sciencedirect.com

ScienceDirect

Procedia CIRP 49 (2016) 163 – 169

www.elsevier.com/locate/procedia

The Second CIRP Conference on Biomanufacturing

Left ventricular assist devices: Impact of flow ratios on the localisation of cardiovascular diseases using computational fluid dynamics

Michael McElroy, Andres Ruiz-Soler, Amir Keshmiri*

School of Engineering, Manchester Metropolitan University, Manchester, M1 5GD, U.K.

** Corresponding author. Tel.: +44(0)161 2471695. E-mail address: a.keshmiri@mmu.ac.uk*

Abstract

The use of Left Ventricular Assistive Devices (LVADs) is increasing for people with heart failure. The present computational fluid dynamics study provides insight into the significance of the flow ratio between the cannula and the aortic root on the prediction of lesion localisation in a typical LVAD configuration, which in turn affects the design and manufacture of these devices. Three cases were studied with varying percentages of flow through the two inlets; the cannula inlet was assumed steady-state, whilst the aortic root inlet had a scaled pulsatile profile, representative of the extent of heart failure. Results suggest that as the flow exiting the heart decreases in velocity, if not orientated properly, the jet exiting the cannula graft can 'obstruct' flow to the innominate, common carotid and left subclavian arteries. Therefore, patients with less severe heart failure will generally experience relatively good perfusion of these arteries. However, for the more severe cases of heart failure, the orientation of the cannula graft should be such that adequate perfusion to the aforementioned arteries is maintained.

Peer-review under responsibility of the scientific committee of The Second CIRP Conference on Biomanufacturing

Keywords: CFD; Biodesign; Left Ventricular Assistive Devices; Hemodynamics; Insertion cannula; Aorta; Boundary conditions.

1. Introduction

Cardiovascular disease causes over 4 million (47%) of all deaths in Europe each year [1]. Ventricular assist devices are an established form of treatment for patients with heart failure and result in clear survival benefit [2–6]. The INTERMACS report showed that, in 2011, roughly 1,800 patients were implanted with LVADs (95% of which were continuous flow pumps), this number is expected to increase over time [7].

A complication post-operative of LVADs is the occurrence of thromboembolic events [8]. Pump thrombosis within the LVAD is not the only origin of emboli, mobilisation of atherosclerotic plaque within the ascending aorta, common carotid and subclavian arteries may also contribute due to high Wall Shear Stress (WSS) [9]. The occurrence and mobilisation of lesions within the ascending aorta is affected by the nature of the outflow cannula placement and function. Therefore, not only is it important to consider unfavourable haemodynamics within the LVAD, but also within the aorta, cannulas, common carotid, innominate and subclavian arteries.

During the implantation of an LVAD, the inflow cannula connects the left ventricle to the LVAD, while the outflow cannula is anastomosed to the right anterior of the ascending aorta. Despite having significant effects on haemodynamics, design and placement of cannulas during both LVAD and Cardio-Pulmonary Bypass (CPB) often varies from surgeon to surgeon. The parameters to consider during cannula placement include:

- *Cannula tip design*: has been shown to have an influence on thrombus formation and mobilisation [10–12]. Altering the end-hole tip design of a diffuser plays a significant role in head-neck perfusion when compared with altering the orientation during CPB [10]. There have been proposed cannula tip designs to improve aortic cannula practice such as a novel four-lobe swirl inducer [10,13]. A diffuser tipped cannula reduces flow velocities and WSS, therefore reducing the risk of mobilising atherosclerotic or thrombotic plaque [10]. A

Peer-review under responsibility of the scientific committee of The Second CIRP Conference on Biomanufacturing
doi:10.1016/j.procir.2015.11.008

group at RWTH Aachen University in Germany have developed a validated Computational Fluid Dynamic (CFD) model to analyse the effect of outflow cannula shape, with the intention of reducing the jet effect and increasing cerebral perfusion during CPB [11,14]. Their work suggests that work needs to be done to determine a velocity threshold associated with plaque mobilisation.

- *Cannula insertion angle and location*: are both also crucial to reducing thrombus formation and mobilisation [10–12] and have been relatively widely studied [15–17]. Insertion angle has a significant effect significant effect on WSS [18] and flow patterns and often leads to thrombosis and emergency surgery for device replacement [19,20]. It is widely accepted that large variations in flow velocities within the ascending aorta are dependent on the angle of the outflow cannula anastomosis relative to the ascending aorta [21,22]. The normal rule is to insert the cannula high up in the ascending aorta, however, it has been shown that positioning the cannula sufficiently far away from the brachiocephalic artery branch may be crucial in reducing backflow [10]. With the exception of [23], there is still some uncertainty as to whether inflow cannula (into the apex of the left ventricle) positioning contributes to the development of thrombosis or not [19], however, this work is more concerned with the impact of haemodynamics within the aorta and it's neighbouring branches, therefore, the inlet cannula configuration will not be discussed any further in this work.
- *Pulsatile/continuous flow from LVAD/CPM machine*: numerical work comparing the difference between pulsatile and continuous flow during CPB has shown that WSS is remarkably higher during pulsatile flow, which may induce arteriosclerotic plaque embolism [9].

Despite there currently being a wide range of research surrounding cannula implantation, to the authors' knowledge, there appears to be no emphasis on the ratio of blood flowing from the aortic root and that from the cannula outlet on the numerical prediction of lesion deposition. This ratio is likely to be highly dependent on the state of HF of the patient. Despite left ventricular function no longer significantly contributing to aortic flow post LVAD placement [24], it is feasible that the ratio between the flow entering the aorta via the LVAD and the native left ventricle has an impact on potential future cardiovascular complications. Therefore, there is scope for work that defines whether or not such a ratio has a significant relationship to the probability of the patient developing cardiovascular complications post LVAD implantation. If such a relationship is found to be important, it may influence the surgeon's decisions during LVAD implantation or CPB surgery.

Therefore, the aim of this work is to quantify the impact associated with prescribing different inlet flow ratios to the aortic root and cannula in an LVAD configuration on the CFD simulation of haemodynamics within the cardiovascular system for predicting the localisation of lesion. It is worth noting that any implications that arise from this study are also applicable to CPB.

2. Method

2.1. Geometrical model

A review by [25] reveals that out of over 5000 patients with continuous-flow (second generation) LVADs, 77.7% were male. For this reason, a patient-specific model of a 23 year old male with normal aortic function was used in this work. The aorta geometry was produced using SimVascular software (Simtk.org) to process Gadolimium-enhanced MRA image data (Open Source Medical Software Corp). The aorta geometry was then combined with a simplified cannula (10mm diameter) geometry of a continuous-flow LVAD (see Figure 1). An arbitrary cannula insertion angle of ≈20 degrees was used. The angle is relative to a surface that crosses through the centre of the anastomosis region and remains tangential to the ascending aorta wall. The cannula geometry was based on a typical continuous-flow LVAD configuration. This basis was chosen because the most common and successful second generation pump worldwide as bridge to transplant and destination therapy is the HeartMate II (Thoratec Corp, Pleasanton, CA, USA), which is a continuous-flow device [26]. The present geometry is representative of the typical configuration of a second generation pump, in which a 10mm diameter cannula is connected to the apex of the left ventricle, with the outflow graft anastomosed to the ascending aorta [26], at an angle such that the flow is directed through the aorta with even flow distribution.

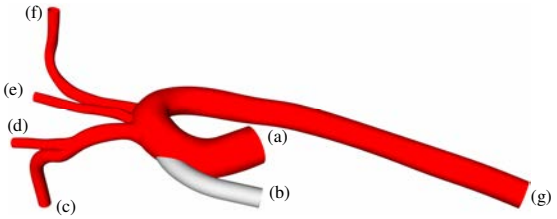

Figure 1. Schematic of the present configuration: an aorta (that of a 23 year old male) with normal aortic function with an LVAD outflow graft connected to the ascending aorta. (a) inlet/aortic root; (b) inlet/cannula graft; (c) outlets/right subclavian artery; (d) outlet/right common carotid artery; (e) outlet/left common carotid artery; (f) outlet/left subclavian artery; (g) outlet/thoracic aorta.

2.2. Computational domain

The geometry was meshed using ICEM-CFD version 15.0. The mesh, which consisted of ≈4.3 million elements was based on a finite volume hybrid mesh consisting of tetrahedral elements within the core region and prism layers (3 elements thick) near the wall to allow for large spatial velocity gradients. In order to ensure the accuracy of the simulations, a series of steady-state computations with different mesh refinement were conducted to ensure grid independency prior to running the present computations. The computational domain with ≈3.8 million tetrahedron and ≈500,000 prism elements were considered to be sufficient here, as further mesh refinement could only result in less than 1% change in velocity and WSS at some examined sections.

2.3. Boundary conditions

In the present work, three cases are studied based on different combinations of inlets, as shown in Table 1. The flow ratios defined in the simulations represent the extent of heart failure of the patient.

Table 1. Summary of cases studied in the present work. Constant cannula flow rates were obtained by time-averaging the healthy pulsatile flow rate and scaling accordingly.

	Flow based on healthy heart flow rate	
	Aortic root (pulsatile)	Cannula (constant)
Test 1	40%	1.60 cm/s, 60%
Test 2	50%	1.34 cm/s, 50%
Test 3	60%	1.07 cm/s, 40%

Steady, uniform mass influx' were imposed over the entire cannula inlet boundary. Due to the pulsatile nature of the heart, a flat, pulsatile velocity waveform based on experimental data by [27] was applied at the aortic root and scaled to 40, 50 and 60% of the normal magnitudes reach by a healthy heart to simulate various extent of HF. The assumption of a flat velocity profile at the aortic inlet has been verified by various *in vivo* measurements using different animal models, which have demonstrated that the velocity profile distal to the aortic valve is essentially flat in the ascending aorta and only consisted of a weak helical component.[27].

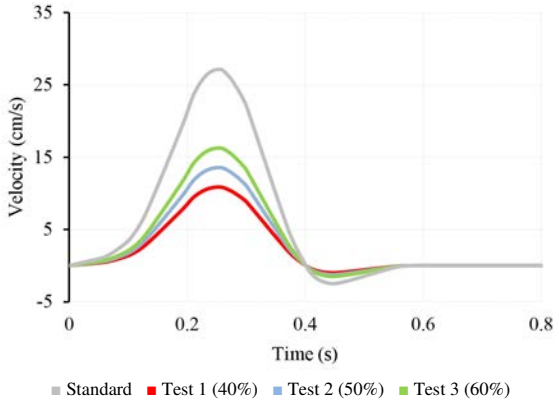

Figure 2. Inlet velocity pulsatile waveforms forms applied at the aortic root. Waveforms have been scaled based on the standard (grey curve) profile taken from experimental data by [27].

Similar to the works of numerous researchers including [27–30], a 'traction free' or 'zero pressure' Boundary Condition (BC) was applied to each outlet. No-slip BC is applied to all walls and a rigid wall model is also assumed, which has been shown to be a valid assumption [31].

2.4. Numerical procedure

Blood flow was defined as a three-dimensional, incompressible, isothermal, and laminar flow, whose governing equations are:

Continuity equation,

$$\nabla \cdot \mathbf{u} = 0 \tag{1}$$

Navier-Stokes equation,

$$\rho \frac{\partial \mathbf{u}}{\partial t} + \rho(\mathbf{u} \cdot \nabla)\mathbf{u} = -\nabla p + \eta \nabla^2 \mathbf{u} \tag{2}$$

where $\boldsymbol{u}$ is the velocity vector, t is the time, p is the pressure, and μ is the dynamic viscosity of blood set to 4.043 g/ms. The density (ρ) of blood is assumed to be 1044 kg/m^3. Non-Newtonian fluid properties of the blood were neglected.

The governing equations are solved numerically by a finite volume method and the CFD code, ANSYS-CFX (Version 15.0), using a fully implicit second-order backward Euler differencing scheme. Each simulation ran for one period (T) of 0.8s, with a time-step size of 0.032s. The convergence criterion (a normalised residual, obtained based on the imbalance in the linearised system of discrete equations) is set to 10^{-5} in this study. Commercial visualisation tool, Ensight (CEI Inc., Research Triangle Park, NC, USA) was used to post-process the results.

3. Results and Discussion

3.1. Haemodynamic parameters

The localisation of various lesions including atherosclerosis, intimal hyperplasia and intimal thickening have been extensively studied and are related to different local haemodynamic metrics [32–34]. These haemodynamic parameters can be directly derived from the flow velocity fields obtained by CFD-based simulation tools. Whilst the performance of these parameters on predicting the localisation of atheroma is important in this study, the focus is on the sensitivity of these parameters to the BCs prescribed during the numerical simulation.

The parameters chosen for the present analyses include WSS, Time-Averaged WSS (TAWSS) [35], TAWSS Gradient (TAWSSG) [36], Oscillatory Shear Index (OSI) [35], and Relative Residence Time (RRT) [37], calculated according to Eqs. (3)-(6), below. These parameters have been chosen because i) localised distribution of low-WSS and high-OSI strongly correlate with the locations of atheroma [35], ii) large spatial TAWSSG contributes to elevated wall permeability and atherosclerotic lesions [38], iii) platelet activation may be induced by the combination of large exposure time and highs shear stress [39–42], iv) stagnant and recirculating flow regions can cause platelet aggregation and thrombogenesis.

$$TAWSS = \frac{1}{T}\int_0^T \left|\vec{\tau}_W\right| dt \tag{3}$$

$$TAWSSG = \frac{1}{T}\int_0^T \sqrt{\left(\frac{\partial \tau_x}{\partial x}\right)^2 + \left(\frac{\partial \tau_y}{\partial y}\right)^2 + \left(\frac{\partial \tau_z}{\partial z}\right)^2}\, dt \quad (4)$$

$$OSI = \frac{1}{2}\left(1 - \frac{\left|\int_0^T \vec{\tau}_W dt\right|}{\int_0^T |\vec{\tau}_W| dt}\right) \quad (5)$$

$$RRT = \frac{1}{(1-2\times OSI)\times TAWSS} = \frac{1}{\frac{1}{T}\left|\int_0^T \vec{\tau}_W dt\right|} \quad (6)$$

Figure 3 shows the distribution of the above metrics for all three tests and in what follows, each hemodynamic metric will be discussed separately:

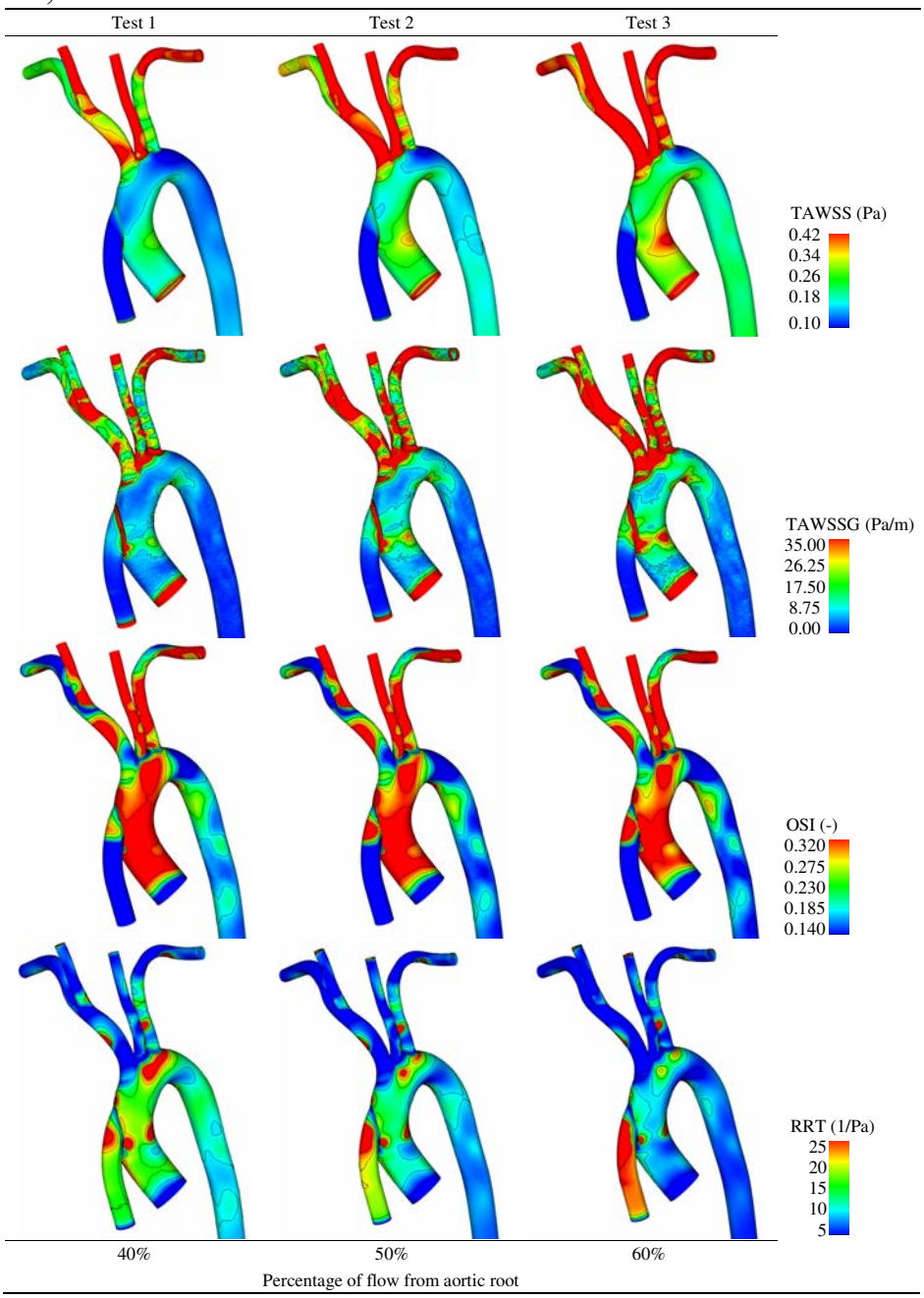

Figure 3. Distributions of different haemodynamic parameters calculated for the aortic arch and descending thoracic aorta, viewed from outside the vessel.

TAWSS: overall, TAWSS values increased when progressing from Test 1 to Test 3, with Tests 2 and 3 experiencing increases of 21% and 44%, respectively when compared to Test 1. With the exception of TAWSS decreasing by 5% and 9% within the cannula graft in Tests 2 and 3, respectively, this is likely caused by the reduced imposed graft inlet velocity.

TAWSSG: values again, progressively increased from Test 1-3, Test 2 (+33%), Test 3 (+71%). Peak magnitudes occurred within the ascending aorta and ascending branches.

OSI: distribution remained relatively unaffected by the imposed flow ratios, with values of +2% and +3% for Tests 2 and 3, respectively, in comparison with Test 1. However, OSI progressively increased within the cannula graft, this is most likely due to the increasing magnitude of the pulsatile flow flowing from the aortic root having more influence on the haemodynamics within the cannula graft as the velocity imposed within the cannula decreases.

RRT: overall, values decrease within the aorta and ascending branches as tests progress (-13% and -20% for Test 1 and Test 2, respectively). The opposite, however, occurs with the cannula graft (+23% and +56% in Test 1 and 2, respectively), this pattern is due to the flow ratios switching over, where the dominant flow effects change from being caused by the cannula to the aortic root flow.

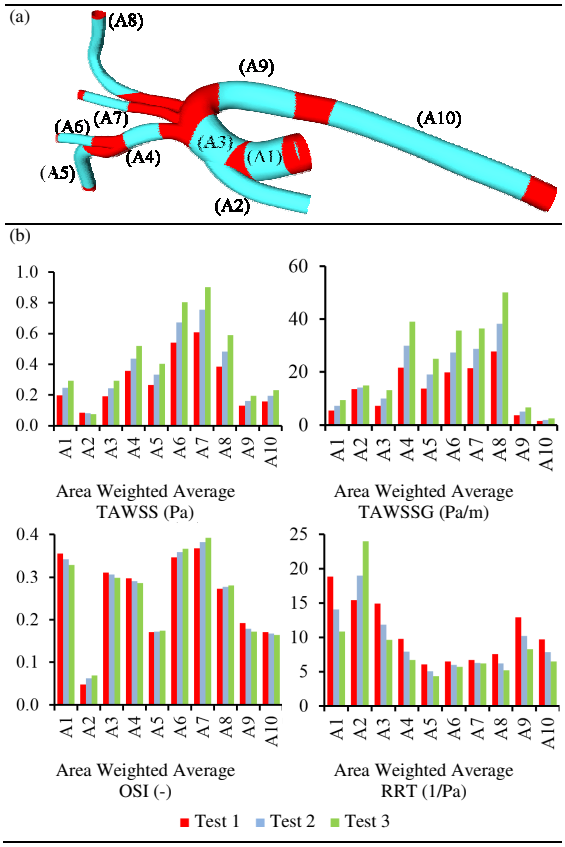

Figure 4. (a) Areas (A) on which area weighted average values are calculated. (b) Charts of area weighted average values of the metrics studied. Specific values for each area are shown in Appendix A.

For more quantitative comparison, Figure 4 shows area-weighted average values of TAWSS, TAWSSG, OSI and RRT evaluated over various locations within the aortic model.

Time-averaged Velocity (TAV) distributions are shown on a monitoring plane within the aortic arch in Figure 5(b). A three-colour contour of TAV is also shown on the same monitoring plane (Figure 5c). Blue and red areas represent WSS<75% and WSS>125% of the average value evaluated over the shown area, respectively. Average values of Tests 1-3 are 2.39, 2.81 and 3.23 cm/s, respectively. This figure suggests that with severe HF (40% of normal function) the high velocity jet from the cannula focuses most of the flow onto the wall directly opposite the cannula anastomosis location. Whilst as the function of the heart increases, the flow from the heart more evenly distributes the flow through the aortic arch.

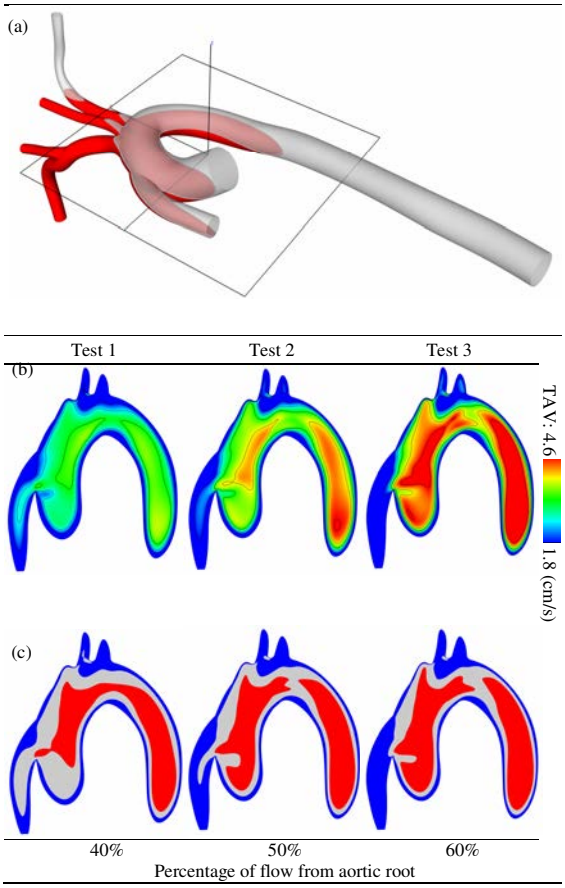

Figure 5. (a) Monitoring place within the aortic arch. (b) Distributions of TAV shown on the monitoring plane. (c) Three-colour contour of TAV shown on the monitoring plane within the aortic arch. Blue and red areas represent TAV<75% and TAV>125% of the average value evaluated over the shown area respectively. Average values of Test 1, Test 2 and Test 3 are 2.39, 2.81 and 3.23 cm/s respectively.

3.2. Limitations of this study

Non-Newtonian fluid properties and fluid-structure interaction were neglected in this study with the intention of explicitly analysing the effects due to the flow split ratio between the cannula and aortic root boundary. However, there are a number of other limitations to this study that will have an effect on explicitly analysing the effects of the flow split ratios, hence, the following limitations offer potential further work:

- The section of geometry consisting of the cannula graft and anastomosis was a simplified model of the normal location, orientation, angle, diameter and curvature. Hence, if MRI obtained geometry of a patient with an implanted LVAD would have been used, the haemodynamics would be more physiologically accurate.
- The results were not validated against *in vivo* data, however, this study aimed to draw attention to this area of research and assess its potential rather than an in-depth and validated analysis.
- Each simulation was ran for one pulse period, ideally, the simulation will run for at least 3 periods, and results are recorded during the final period, this is to allow any start-up effects to be negated.
- To reduce solution time, the time increment in this study was relatively large, reducing the increment size would produce more accurate and stable results. However, the time increment size was found to be fair as it produced realistic results and this work is intended as a preliminary study to investigate this area's worthiness of further study.
- As alluded to earlier, research concerning the implantation of LVAD outflow cannula is also applicable to CPB to some degree, and vice versa. However, it is worth noting that the velocity from the cannula returning blood during CPB is often significantly higher than LVADs, thus increasing the risk of dislodging parts of atherosclerotic lesions, creating an emboli, which can ultimately result in stroke [10]. The results in this study are not representative of such a high jet velocity as it is focused on the flow from an LVAD.

4. Conclusion

These results suggest that patients with less severe extent of HF will generally experience good perfusion of innominate, common carotid and left subclavian arteries, however, for the more severe cases of HF, the orientation of the graft anastomosis should be such to maintain adequate perfusion to these arteries, as the flow exiting the heart decreases, if not orientated properly, the jet of the cannula graft can 'obstruct' flow to the aforementioned arteries.

This work does however require more extensive investigation to more reliably define the effects flow ratios between the cannula jet and the heart output have on the deposition of CVDs, particularly; results require validation against *in vivo* data; finer time step sizes and a greater number of time periods.

This work is a good preliminary study for further investigation into the optimal combination of cannula tip design and cannula location relative to the condition of the patient. The data from such a study could prove useful for pre-operative planning, whether the patient has total or partial HF, the data will be able to direct the surgeon to an optimal surgical strategy in order to reduce post-operative risk of CVDs.

Acknowledgements

The authors would like to thank Dr Glen Cooper and Prof Neil Reeves for their support throughout this work along with the Manchester Metropolitan University School of Engineering for funding this research.

Appendix A. Area weighted average values of metrics studied

Table 2. Area weighted average values of TAWSS, TAWSSG, OSI and RRT evaluated over various locations shown in Figure 4.

	Area	TAWSS			TAWSSG			OSI			RRT		
		Test 1 (Pa)	Test 2 (%)	Test 3 (%)	Test 1 (Pa/m)	Test 2 (%)	Test 3 (%)	Test 1 (-)	Test 2 (%)	Test 3 (%)	Test 1 (1/Pa)	Test 2 (%)	Test 3 (%)
Aortic Root	A1	0.2	+24.2	+48.0	5.4	+36.2	+76.4	0.4	-3.6	-7.6	18.8	-25.5	-42.5
Graft	A2	0.1	-4.8	-8.8	13.5	+4.5	+11.5	0.0	+30.1	+46.5	15.4	+23.3	+55.6
Ascending Aorta	A3	0.2	+25.6	+52.2	7.3	+35.7	+78.1	0.3	-1.5	-3.9	15.0	-20.8	-35.7
Innominate Artery	A4	0.4	+22.5	+45.9	21.7	+37.5	+79.5	0.3	-2.2	-3.7	9.8	-18.8	-31.3
Right Subclavian Artery	A5	0.3	+25.3	+51.9	13.8	+38.3	+80.7	0.2	+0.2	+1.6	6.1	-17.3	-28.4
Right Common Carotid Artery	A6	0.5	+24.3	+48.9	19.9	+37.6	+79.1	0.3	+3.7	+5.8	6.4	-7.4	-12.0
Left Common Carotid Artery	A7	0.6	+24.0	+48.4	21.4	+34.3	+70.4	0.4	+3.8	+6.8	6.7	-5.8	-7.3
Left Subclavian Artery	A8	0.4	+25.9	+53.8	27.8	+37.5	+79.9	0.3	+1.3	+2.8	7.6	-18.6	-31.0
Descending Aorta	A9	0.1	+22.9	+49.0	3.7	+35.7	+77.9	0.2	-6.8	-10.4	12.9	-21.3	-35.9
Thoracic Aorta	A10	0.2	+23.4	+47.5	1.5	+33.5	+71.7	0.2	-2.0	-3.7	9.7	-19.7	-33.4

References

[1] Nichols M, Townsend N, Scarborough P, Rayner M. European

cardiovascular disease statistics. 2012.
[2] Trachtenberg BH, Cordero-Reyes A, Elias B, Loebe M. A review of infections in patients with left ventricular assist devices: prevention, diagnosis and management. Methodist Debakey Cardiovasc J 2015:28–32.
[3] Slaughter MS, Rogers JG, Milano CA, Russell SD, Conte J V, Feldman D, et al. Advanced heart failure treated with continuous-flow left ventricular assist device. N Engl J Med 2009;361:2241–51.
[4] John R, Kamdar F, Liao K, Colvin-Adams M, Boyle A, Joyce L. Improved Survival and Decreasing Incidence of Adverse Events With the HeartMate II Left Ventricular Assist Device as Bridge-to-Transplant Therapy. Ann Thorac Surg 2008;86:1227–35.
[5] John R, Kamdar F, Eckman P, Colvin-Adams M, Boyle A, Shumway S, et al. Lessons learned from experience with over 100 consecutive HeartMate II left ventricular assist devices. Ann Thorac Surg 2011;92:1593–600.
[6] Kirklin JK, Naftel DC, Kormos RL, Stevenson LW, Pagani FD, Miller M a., et al. The Fourth INTERMACS Annual Report: 4,000 implants and counting. J Hear Lung Transplant 2012;31:117–26.
[7] Kirklin JK, Naftel DC, Kormos RL, Stevenson LW, Pagani FD, Miller M a, et al. Fifth INTERMACS annual report: risk factor analysis from more than 6,000 mechanical circulatory support patients. J Heart Lung Transplant 2013;32:141–56.
[8] Menon AK, Götzenich A, Sassmannshausen H, Haushofer M, Autschbach R, Spillner JW. Low stroke rate and few thrombo-embolic events after HeartMate II implantation under mild anticoagulation † 2012;42:319–23.
[9] Lux P, Akhyari P, Boeken U, Assmann A, Cemal A, Fethi G, et al. Pulsatile extracorporeal circulation during on-pump cardiac surgery enhances aortic wall shear stress 2012;45:156–63.
[10] Menon PG, Antaki JF, Undar A, Pekkan K. Aortic outflow cannula tip design and orientation impacts cerebral perfusion during pediatric cardiopulmonary bypass procedures. Ann Biomed Eng 2013;41:2588–602.
[11] Kaufmann TAS, Schlanstein P, Moritz A, Steinseifer U. Development of a Hemodynamically Optimized Outflow Cannula for Cardiopulmonary Bypass. Artif Organs 2014.
[12] White JK, Jagannath A, Titus J, Yoneyama R, Madsen J, Agnihotri AK. Funnel-tipped aortic cannula for reduction of atheroemboli. Ann Thorac Surg 2009;88:551–7.
[13] Menon PG, Teslovich N, Chen C-Y, Undar A, Pekkan K. Characterization of neonatal aortic cannula jet flow regimes for improved cardiopulmonary bypass. J Biomech 2013;46:362–72.
[14] Kaufmann TAS, Wong KC, Schmitz-Rode T, Steinseifer U. Mimicking of cerebral autoregulation by flow-dependent cerebrovascular resistance: a feasibility study. Artif Organs 2012;36:E97–101.
[15] Laumen M, Kaufmann T, Timms D, Schlanstein P, Jansen S, Gregory S, et al. Flow analysis of ventricular assist device inflow and outflow cannula positioning using a naturally shaped ventricle and aortic branch. Artif Organs 2010;34:798–806.
[16] Kaufmann TAS, Hormes M, Laumen M, Timms DL, Linde T, Schmitz-Rode T, et al. The impact of aortic/subclavian outflow cannulation for cardiopulmonary bypass and cardiac support: a computational fluid dynamics study. Artif Organs 2009;33:727–32.
[17] May-Newman K, Hillen B, Dembitsky W. Effect of left ventricular assist device outflow conduit anastomosis location on flow patterns in the native aorta. ASAIO J 2006;52:132–9.
[18] May-Newman K, Hillen B, Sironda CS, Dembitsky W. Effect of LVAD outflow conduit insertion angle on flow through the native aorta. J Med Eng Technol 2004;28:105–9.
[19] Bhama J, Eckert C, Lockard K, Shiose A, Bermudez C, Teuteberg J, et al. Does Lvad Inflow Cannula Position Contribute To the Development of Pump Thrombosis Requiring Device Exchange? J Am Coll Cardiol 2013;61:E719.
[20] Ammar KA, Umland MM, Kramer C, Sulemanjee N, Jan MF, Khandheria BK, et al. The ABCs of left ventricular assist device echocardiography : a systematic approach 2012:1–15.
[21] Dalby M, Banner N, Tansley P. Left ventricular function during support with an asynchronous pulsatile left ventricular assist device. J Hear Lung Transplant 2003;2498:292–300.
[22] Karmonik C, Partovi S, Schmack B, Weymann A, Loebe M, Noon GP, et al. Comparison of hemodynamics in the ascending aorta between pulsatile and continuous flow left ventricular assist devices using computational fluid dynamics based on computed tomography images. Artif Organs 2014;38:142–8.
[23] Ong C, Dokos S, Chan B, Lim E, Al Abed A, Bin Abu Osman NA, et al. Numerical investigation of the effect of cannula placement on thrombosis. Theor Biol Med Model 2013;10:35.
[24] Oz M, Argenziano M, Catanese KA, Gardocki MT, Goldstein DJ, Ashton RC, et al. Bridge experience with long-term implantable left ventricular assist devices. Are they an alternative to transplantation? Circulation 1997;95:1844–52.
[25] Xie A, Phan K, Yan TD. Durability of continuous-flow left ventricular assist devices: a systematic review. Ann Cardiothorac Surg 2014;3:547–56.
[26] Garbade J, Bittner HB, Barten MJ, Mohr F. Current Trends in Implantable Left Ventricular Assist Devices 2011;2011:18–22.
[27] Caballero a. D, Laín S. A Review on Computational Fluid Dynamics Modelling in Human Thoracic Aorta. Cardiovasc Eng Technol 2013;4:103–30.
[28] Vignon-Clementel IE, Figueroa CA, Jansen KE, Taylor CA. Outflow boundary conditions for 3D simulations of non-periodic blood flow and pressure fields in deformable arteries. Comput Methods Biomech Biomed Engin 2010;13:625–40.
[29] Taylor CA, Figueroa CA. Patient-specific modeling of cardiovascular mechanics. Annu Rev Biomed Eng 2009;11:109–34.
[30] Moon JY, Suh DC, Lee YS, Kim YW, Lee JS. Considerations of Blood Properties, Outlet Boundary Conditions and Energy Loss Approaches in Computational Fluid Dynamics Modeling. Neurointervention 2014;9:1–8.
[31] Moore Jr JE, Maier SE, Ku DN, Boesiger P. Hemodynamics in the abdominal aorta: a comparison of in vitro and in vivo measurements. J Appl Physiol 1994;76:1520–7.
[32] Archie JP, Hyun S, Kleinstreuer C, Longest PW, Truskey GA, Buchanan JR. Hemodynamic parameters and early intimal thickening in branching blood vessels. Crit Rev Biomed Eng 2001;29:1–64.
[33] Steinman DA. Image-based computational fluid dynamics: A new paradigm for monitoring hemodynamics and atherosclerosis. Curr Drug Targets - Cardiovasc Haematol Disord 2004;4:183–97.
[34] Ghista DN, Kabinejadian F. Coronary artery bypass grafting hemodynamics and anastomosis design: a biomedical engineering review. Biomed Eng Online 2013;12:129.
[35] He X, Ku DN. Pulsatile flow in the human left coronary artery bifurcation: Average conditions. J Biomech Eng 1996;118:74–82.
[36] Buchanan JR, Kleinstreuer C, Hyun S, Truskey GA. Hemodynamics simulation and identification of susceptible sites of atherosclerotic lesion formation in a model abdominal aorta. J Biomech 2003;36:1185–96.
[37] Lee S-W, Antiga L, Steinman DA. Correlations among indicators of disturbed flow at the normal carotid bifurcation. J Biomech Eng 2009;131:061013.
[38] DePaola N, Gimbrone MA, Davies PF, Dewey CF. Vascular endothelium responds to fluid shear stress gradients. Arter Thromb Vasc Biol 1992;12:1254–7.
[39] Hellums JD. Whitaker lecture: Biorheology in thrombosis research. Annals of Biomedical Engineering. Ann Biomed Eng 1993;22:445–55.
[40] Ramstack JM, Zuckerman L, Mockros LF. Shear-induced activation of platelets. J Biomech 1979;12:113–25.
[41] Wurzinger LJ, Opitz R, Eckstein H. Mechanical bloodtrauma. An overview. Angeiologie 1986;38:81–97.
[42] Wurzinger L, Optiz R, Wolf M, Schmid-Schonbein H. Shear induced platelet activation - a critcal reappraisal. Biorheology 1985;22:399–413.